

Full Paper

PE/PET Li-ion Battery Separator: Preparation by Wet Method and Electrospinning and Its Comparison with Industrial PP Separator

Ramin Badrnezhad,¹ Abolfazl Fathollahi Zonouz,² and Hamed Pourfarzad^{3,*}

¹*Department of Chemistry and Chemical Engineering, Malek-Ashtar University of Technology, Tehran, P.O. Box 15875-1774, Iran*

²*Organic Polymer Chemistry Research Laboratory, Department of Chemistry, University of Isfahan, Isfahan, Iran*

³*Center of Excellence in Electrochemistry, University of Tehran, Tehran, Iran*

*Corresponding Author, Tel.: +989100998568

E-Mail: H.Pourfarzad2030@gmail.com

Received: 2 August 2021 / Received in revised form: 9 February 2022 /

Accepted: 12 February 2022 / Published online: 28 February 2022

Abstract- Lithium-ion batteries (LIB) have attracted enormous attention in the past decades due to their outstanding features, such as high energy density, long cycle life, low self-discharging capacity. Although Lithium-ion batteries have been an energy storage system for commercial electronics, issues regarding its safety raised doubt about its usage for energy storage. This paper presents a bilayer Li-ion battery separator produced by the wet method for its Polyethylene (PE) base layer, which has been reinforced by a nonwoven polyethylene terephthalate layer by electrospinning. This separator has appropriate porous morphology, 41% porosity, BET specific surface area of 39.3 m²/gr, an average pore diameter of 22 nm, electrolyte uptake of 216%, a tensile strength of 100 MPa, the ionic conductivity of 0.451 mS/cm, Excellent electrochemical stability up to 4.6 volts, acceptable cyclic performance and charge and discharge capacity which provides the expected characteristics of a suitable separator and, above all, due to the presence of a layer PET provides a shutdown safety window of about 100 degrees Celsius by improving its dimensional stability under high temperatures.

Keywords- Li-ion battery; Polyethylene; Polyethylene terephthalate; Separator; Shutdown

1. INTRODUCTION

Lithium-ion batteries (LIB) have attracted enormous attention in the past decades due to their outstanding features, such as high energy density, long cycle life, low self-discharging capacity. The separator plays a crucial role in Li-ion batteries by physically separating the cathode and anode to avoid the short-circuit, and at the same time, allowing the transport of lithium-ion between electrodes [1-3]. Polyolefins such as polyethylene (PE) or polypropylene (PP) are mainly used for producing commercialized separators. In such batteries, short circuit of electrodes caused by thermal shrinkage of separators, and the accelerated LIB reactions due to the increased kinetic reaction rate at higher temperature leads to a further rise of temperature which aggravates this process and may result in severe accidents, such as ignition or explosion. This shows how important it is to find a solution to improve the safety of Li-ion batteries. Enabling thermal shutdown property is one of the practical approaches, which includes using a fusible layer for blocking membrane pores after melting beside another robust layer for maintaining the dimensional stability at high temperature [2-8].

Extensive research has been done in recent years on the different methods of preparation of the Li-ion battery separators and their ability to shut down [9-23]. Tabatabai et al. [23] prepared monolayer and multilayer membranes from PP and HDPE by dry extrusion method. According to their results, at high cold stretching extensions, the pore size and porosity of the HDPE membranes was much larger compared to those from the PP produced under the same conditions. This was attributed to the longer tie chains in the HDPE membranes compared to the PP. In another study, Hao et al. [24] prepared PET fibrous separator. Their results show that these separators have high thermal and porosity resistance and exhibit excellent electrochemical stability, mechanical resistance, and ionic conductivity, so they are suitable for use in lithium-ion batteries. Results of Shi et al. [25] revealed that blending PE-b-PEG into porous HDPE membranes could efficiently improve the performances of PE separators for lithium batteries. Park et al. [26] also developed polyethylene-based separators by the TIPS (Thermally Induced Phase Separation) method using trimethylolpropane tris(2-ethyl hexanoate)(TEPTEH) as a diluent. Wang et al. [8] used di-iso-decyl phthalate as a diluent to prepare the porous membrane of HDPE by the TIPS method. Liao et al. [27] also made HDPE/methylcellulose separator by the TIPS method using dioctyl phthalate (DOP) as diluent. Li et al. [28] also fabricated PP/PE multilayer separators via the combination of multilayer coextrusion and CaCO₃ template method.

Kim et al. [12] showed that the irradiated separator has better thermal shrinkage resistance than the non-irradiated one because of the cross-link of polyethylene formed by gamma-ray irradiation. Moreover, the temperature difference between shutdown and melting integrity of the irradiated separators is increased about two times in comparison with that of the non-irradiated separator. Gao et al. [22] modified PE separator chain structure through the solid-state ultraviolet (UV) irradiation method to achieve a separator with a composite structure of

40% crystallized PE and 70% gel content. Their results demonstrated that the single-layer PE separator could have both auto-shutdown capacity and satisfactory thermal stability after its chain structure is modified; moreover, the heat resistance temperature can be as high as 220°C. In another study, Kim et al. [13] demonstrated that coating polyethylene on the surface of nonwoven PET separators by a simple dip-coating process is useful in adding shutdown functionality and enhancing thermal shrinkage at higher temperatures.

In the present study, a polyethylene separator was prepared by the wet method, and after confirming the morphology necessary for use as a separator in lithium-ion batteries, the possibility of shutdown by PET electrodeposition was investigated. The purpose of this innovative approach was to use the long-distance melting point of the two polymers to provide better immunity and better surface properties of PET to improve battery performance.

2. EXPERIMENTAL SECTION

2.1. Materials

High-density polyethylene (HDPE EX5) and polyethylene terephthalate (PET TG-620S) were purchased from Marun and Shahid Tondguyan Petrochemical Companies (Iran), respectively. Dioctyl phthalate under the IUPAC name of bis(2-ethylhexyl)phthalate as a diluent for PE separator preparation, dichloromethane, and trifluoroacetic acid as solvents for PET were obtained from Merck, Germany. All chemicals were used as received. Dry-method-made Polypropylene (PP) separator (Shenzhen Senior, China) was used as an industrial sample for comparison.

2.2. Preparation of PE separator

Coperion ZSK25 twin-screw extruder was used to mix the DOP diluent with the polymer matrix. The temperature of the extruder zones was adjusted linearly from 170 to 190°C, and the screw speed was set to 60 rpm. 45wt.% of DOP was used as diluent. The resulting melt was collected and then transformed into granules using a granulator. The resulting granules were heated to 170°C by the hot press, and the films were then soaked in ethanol for 24 h to remove DOP and make porosity. To remove residual ethanol, samples were dried in a vacuum oven at 70°C. The final film was stretched by 50% in both directions to achieve the final thickness and sufficient porosity.

2.3. Enabling Shutdown property by electrospinning

For this purpose, the solution of polyethylene terephthalate at concentrations of 20, 23, and 26wt.% was dissolved in a mixture of trifluoroacetic acid and dichloromethane at a 2:8 ratio for electrospinning. After determining the optimum conditions for electrospinning, to complete the fabrication of the PE/PET bilayer separator, the wet-method-made PE separator was placed

as a substrate on the electrospinning collector plate, and nonwoven PET was coated on PE. After about 15 min of electrospinning, approximately 10 μ m of PET was added to the initial 20 μ m PE film thickness, and a less than 30 μ m thick bilayer PE/PET film was obtained.

2.4. Characterization

The porosity of the samples was measured by the Wang method. According to this method, the separator was weighed before and after of 24-hour immersion in n-butanol and calculated according to the following Eq. (1):

$$A_k = \frac{(w_0 - w)\rho_0}{\rho_0 w_0 + (\rho - \rho_0)w} \times 100 \quad (1)$$

where A_k is the percentage of useful porosity, w is the dry separator weight, w_0 is the weight of separator after immersion, ρ and ρ_0 are densities of polyethylene, and n-butanol, respectively. The SERON-AIS2100 scanning electron microscope from South Korea was used to study the porosity morphology of the specimens. All images were taken at 15 kV electron irradiation. For this purpose, the surface of the films was coated with gold.

Average pore diameter and surface area of membranes were determined by Brunauer–Emmett–Teller (BET) test using continuous-flow gas (N_2) adsorption apparatus (BELSORP MINI II, Japan). Degassing of samples was carried out by BELPREP VAC II at 60 °C for 2 hours. The electrolyte uptake was determined by weighing the samples dry and after immersion for 24 h in a liquid electrolyte. The percentage of adsorption is obtained by the Eq. 2:

$$A = \frac{W_{as} - W_{bs}}{W_{bs}} \times 100 \quad (2)$$

where A is the electrolyte uptake, W_{as} and W_{bs} are the separator weights after and before immersion, respectively.

To investigate the stability of the dimensions of the separator under heat against shrinkage, the dimensions of the specimen were measured after storage for 30 minutes at different temperatures, and the percentage of shrinkage was calculated by Eq. 3:

$$S = \frac{A_f - A_i}{A_i} \times 100 \quad (3)$$

where S is the percent of thermal shrinkage, A_f and A_i are the final and initial area of the sample, respectively.

Tensile tests were carried out using Santam tensile machine (Iran) under room temperature (25 °C) with a crosshead speed at 5 mm/min, according to the ASTM D638 standard. Prior to testing, the samples were dried in a vacuum oven at 60 °C for two hours and kept in sealed

desiccators until tests. All the reported values were obtained by averaging over five specimens for each composition.

The melting behavior of the specimens was studied by differential scanning calorimetry (DSC) using the Mettler Toledo DSC1 (Switzerland). Samples were heated in the range of 25-200 °C using a heating rate of 10 °C/min, and the first heating curves were recorded. All DSC measurements were performed under a nitrogen atmosphere, and the weight of each sample was about 7 mg.

Leica DRMX Polarized Optical Microscope (Germany) was used to investigate the initial morphology of electrospun PET fibers to optimize the conditions of the electrospinning process. Images were shut after 5 minutes of electrospinning for each condition.

To determine the ionic conductivity by the electrochemical impedance spectroscopy (EIS), separators were soaked in a liquid electrolyte (one molar lithium hexafluorophosphate (LiPF₆) solution in ethyl carbonate/dimethyl carbonate solvent at a ratio of 1:1) in an Ar-filled glovebox, then were sandwiched between two stainless steel electrodes and assembled a test cell. Samples were tested over the frequency range of 1 Hz to 100 kHz under an AC voltage of 5 mV at room temperature using the OrigaFlex OGF500 (France). Ionic conductivity obtained by Eq. 4:

$$\delta = \frac{d}{RA} \quad (4)$$

where δ is the ionic conductivity, d is the thickness of the separator, A is the electrode area, and R is the bulk resistance.

The electrochemical stability test was performed by linear scanning voltammetry at a scanning rate of 5 mV/s over the voltage range of 2-7 volts using stainless steel and lithium electrodes in a test cell by the Origa Flex OGF500 (France) tester.

Battery performance tests of the membranes were conducted by assembling the unit cell via sandwiching the separator wetted by the liquid electrolyte between graphite and lithium electrodes. The discharge capacity, cycle performance, and rate performance of cells were measured on a Neware Battery Testing System (China) in the voltage window of 0.02-3 V at ambient conditions. The charge and discharge cycling tests were performed at a current density of 0.2 C for 50 cycles, and the C-rate capability measurements were performed at the current rates of 0.1C, 0.2C, 0.5C, and 1C. The shutdown properties of the separators were obtained using the Hioki 3560C ACH itester by measuring their impedance at 1 kHz. The aforementioned test cells were connected to the impedance tester and placed in a temperature-controlled oven at room temperature. The temperature was then increased at a rate of 2°C/min, and the impedance was recorded every 10 s.

3. RESULTS AND DISCUSSION

3.1. Properties of Base PE Separator

The results of the porosity test showed that the base PE separator had 41% porosity. According to references [2,4,29,30], this amount of porosity is suitable for use in lithium-ion batteries. Figure 1 shows the SEM images of the samples produced by the wet method. According to these images, the nanometer-sized porosity is well established in the samples and has a good distribution. These images illustrate the characteristic morphology of the porous films produced by the wet method.

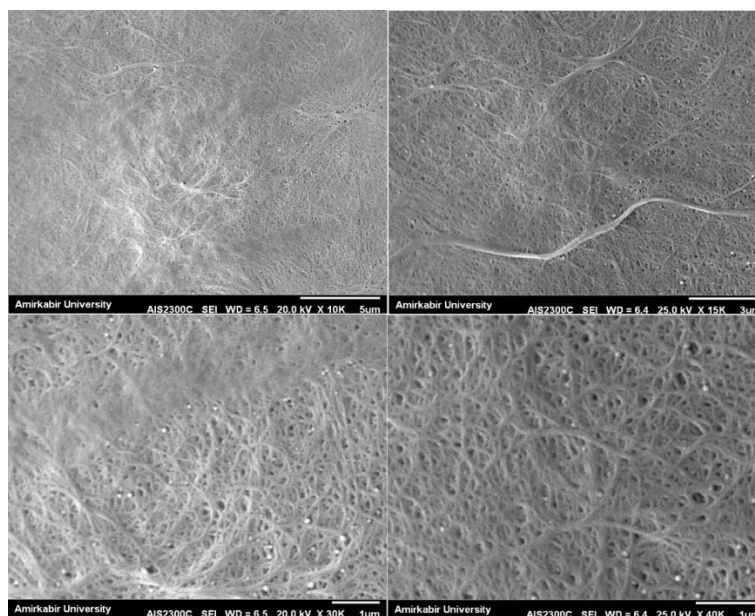


Figure 1. SEM images of PE separator prepared by wet method

For the quantitative determination of specific surface area and pore size, the BET test was performed on PE and PP industrial samples for comparison. Figures 2 and 3 show the diagrams for this test. The hysteresis loop during the adsorption and desorption process is the characteristic behavior of the porous structures, which is clearly shown in the diagram of volume absorbed versus partial pressure in Figure 2. Figure 3 shows the size of the pores and their distribution in the PE separator compared to the Shenzhen Senior PP industrial separator. According to this graph, the decrease in the porosity size in the PE diagram showed a more appropriate pore size distribution of this sample than that of the industrial PP sample. The results of these graphs, together with the corresponding results for the reference Celgard separator[31], are shown in Table 1. According to the final results reported in Table 1 of the BET test, the polyethylene sample produced in this study had a higher level than the PP industrial sample and is close to the Celgard sample. Also, the mean diameter of the pores in

the PE sample is smaller than that of the PP and Celgard samples. These results, along with the results from previous tests, confirm the quality of the primary separator produced in this study.

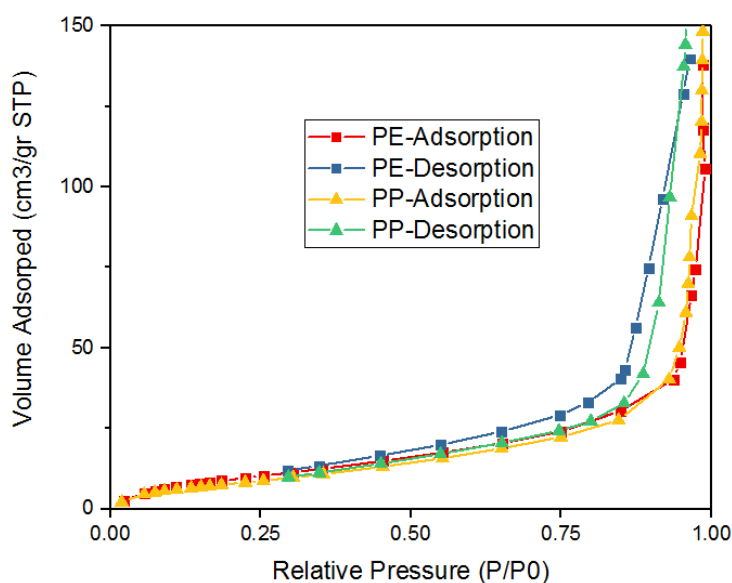


Figure 2. Nitrogen adsorption and desorption isotherms of PE and PP separators

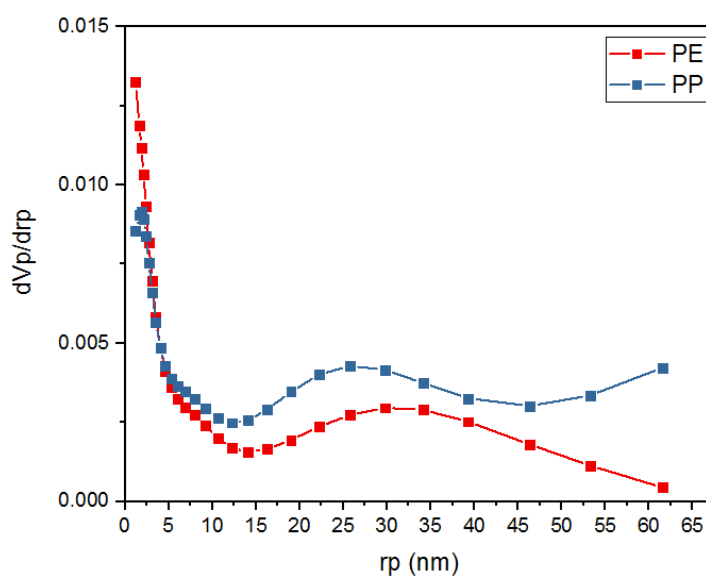


Figure 3. Pore size distribution curves of PE and PP separators

Table 1. Results of BET test

Sample Name	BET Surface Area)m ² /gr(Average pore diameter (nm)
PE	39.3	22
PP-Shenzhen	32.2	31
PP-Celgard 2400 [31]	41.7	26

3.2. Morphology of Electrospun PET

To study the conditions of polyethylene terephthalate electrospinning, the solution containing this polymer at concentrations of 20, 23 and 26wt.% were dissolved in a mixture of trifluoroacetic acid and dichloromethane at a 2:8 ratio, and the optimum parameters for this process were obtained by changing the conditions and examination of the initial morphology by Polarized Light Microscope (POM) images. Table 2 shows these parameters and their values. Initial images obtained POM are shown in Figure 4. The field scanning electron microscopic (FE-SEM) examination was performed to investigate the morphology of the final electrospun samples. Figures 5 to 7 show the FE-SEM images of these samples. According to the FE-SEM images and the average fiber sizes, the 23wt.% solution was selected as the optimum sample, and the optimum conditions were completed.

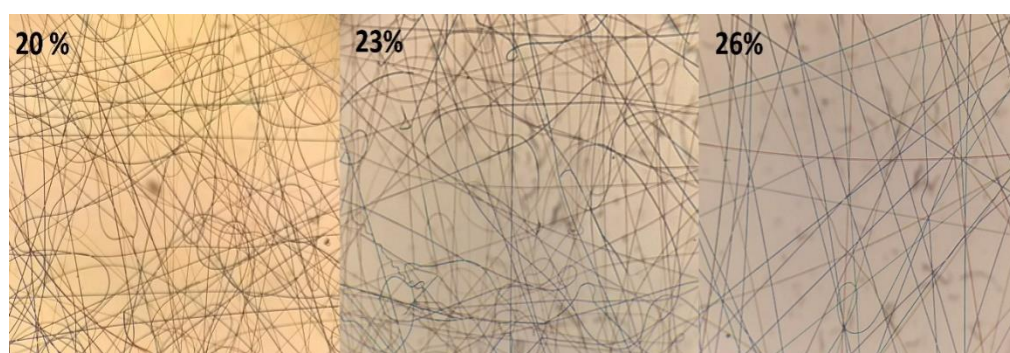


Figure 4. POM images of electrospun PET

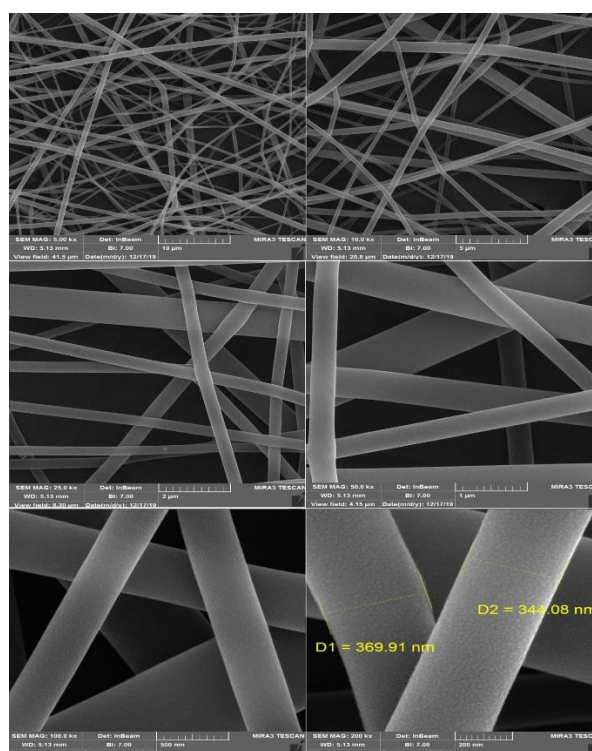


Figure 5. FE-SEM images of 20 wt.% PET electrospun mat

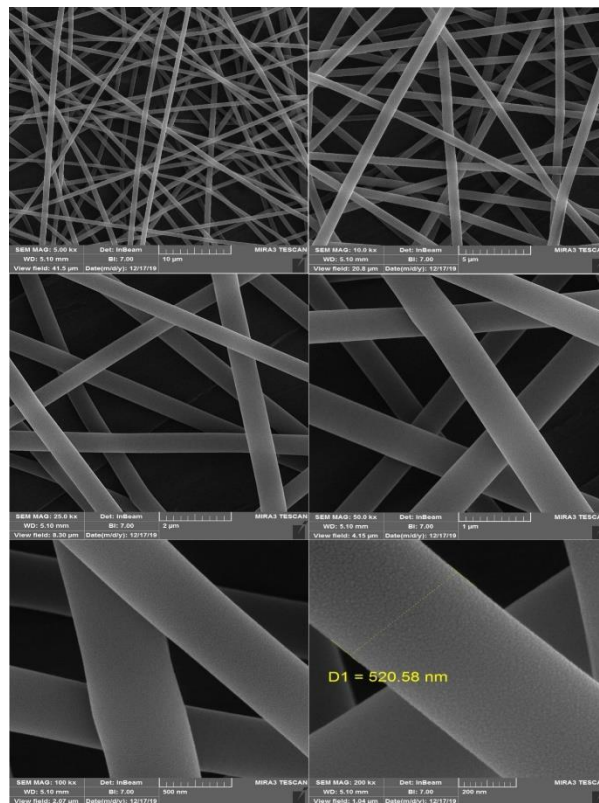


Figure 6. FE-SEM images of 23 wt.% PET electrospun mat

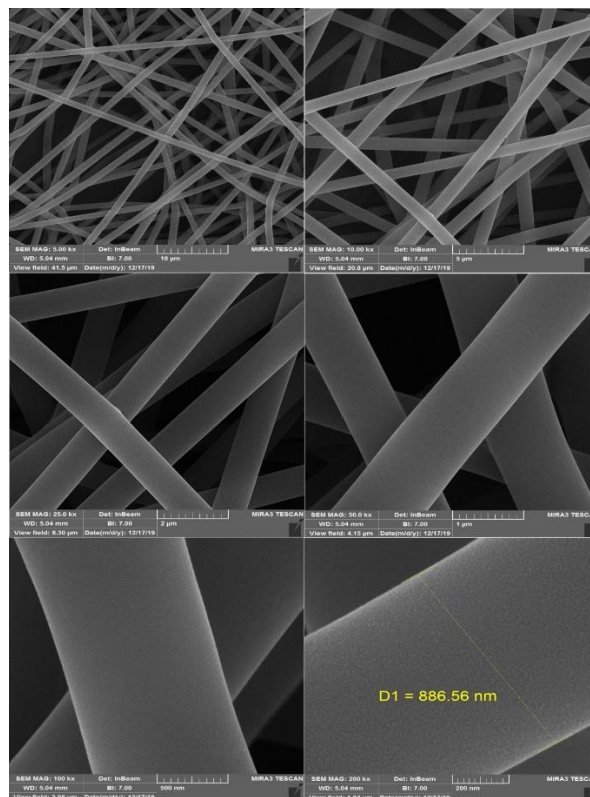


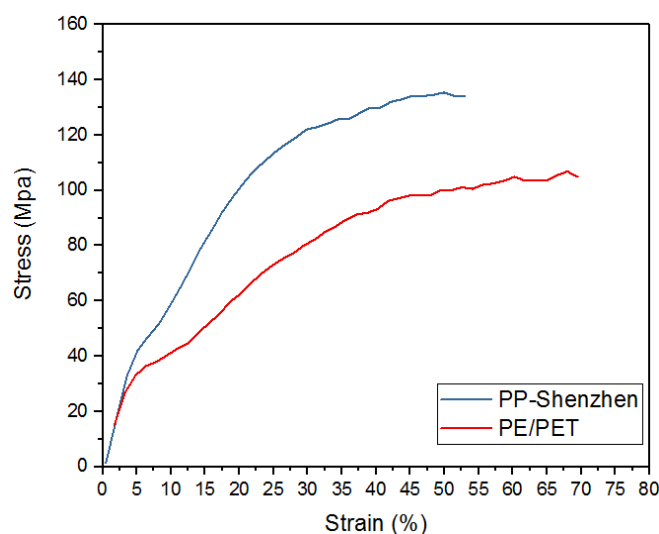
Figure 7. FE-SEM images of 26 wt.% PET electrospun mat

Table 2. Optimal parameters of electrospinning of PET

Parameter	Value	Unit
Voltage	6	kV
The distance between the needle tip and the collector	16	cm
Flow rate	0.4	ml/hr.
Concentration of PET solution	23	wt.%

3.3. Membrane Properties of PE/PET Separator

The electrolyte uptake of the PP industrial sample and PE/PET optimum sample were measured by the gravimetric method. The results of this test are shown in Table 3. These results show that the PE/PET bilayer sample absorbs approximately twice as much as the industrial PP sample. The reason for this can be the increase in hydrophilicity and the improvement of the wettability due to the presence of the PET layer. Since PP and PE are highly nonpolar, the presence of more polar polymer (PET) improves the interaction with the electrolyte and increases the rate of electrolyte uptake. Such an increase is also expected to enhance ion conductivity.

**Figure 8.** Tensile curves of PE/PET and PP separators**Table 3.** Electrolyte uptake test results

Sample	Weight before soaking (mg)	Weight after soaking (mg)	Electrolyte uptake (%)
PP-Shenzhen	3.7	7.8	110
PE/PET	3.0	9.5	216

Figure 8 shows the stress-strain diagram for the industrial PP and PE/PET bilayer separators. According to this graph, although both separators have very close mechanical modulus, the mechanical strength of the PP industrial sample and strain percentage of PE/PET sample are higher. The reason for this can be traced back to the differences in raw materials and production methods. In terms of raw material differences, the polymer PP is stronger than PE, so part of the strength difference between the two samples is due to the inherent strength difference between PP and PE. The second difference, which can be deduced from the strain percentage of these two samples, is the amount of tension applied to the fabrication process. Since the industrial PP sample is made by the dry method, the amount of extension applied during this process has caused the strain-induced crystallization in the tensile direction. This increases the tensile strength while decreasing electrolyte absorption with increasing crystallinity. The higher the crystallinity, the stronger the strength and the lower the strain percentage, which corresponds to the above analysis in the graph. If the tensile strength of the porous PE substrate is increased during the manufacturing process, the strength of this separator will also be increased but will reduce the strain percentage and sacrifice high electrolyte absorption. Also, a comparison of the strength of this sample (about 100 MPa) with the values reported in [2,32] shows that this value is sufficient.

3.4. Thermal and Shutdown Properties of PE/PET Separator

Differential scanning calorimetry tests were performed on different samples to compare the temperature range of the melting and separator shutdown safety. Figure 9 shows the results of this test. According to this diagram, PE melted at a temperature of about 133°C, at which simultaneously lost porosity and mechanical integrity.

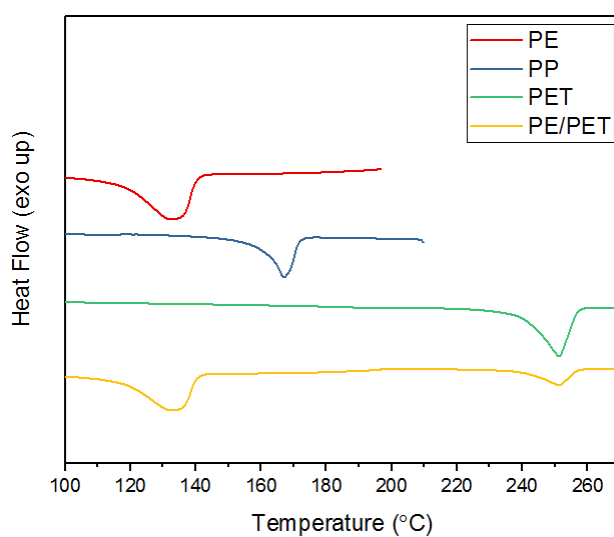


Figure 9. DSC curves of PE/PET and PP separators and PE and PP granules

The industrial PP separator also melted at a temperature of about 167°C and became a non-porous mass. For the PE / PET sample, the graph shows a range of about 120 degrees between PE melting and PET melting. Compared to PP/PE multilayer films with a gap of about 30 to 40 degrees between PE melting (pore closure) and PP melting (loss of mechanical integrity) [19,28], PE/PET melting behavior means much more safety during the shutdown. Despite such distance, the battery stops at about 120 °C with the onset of PE melting, and due to PET melting at about 250°C, the safe temperature range is sufficiently high to maintain mechanical integrity, which prevents the possible occurrence of thermal runaway and explosion.

To evaluate the shrinkage and melting under high temperatures, the separators were placed between the two glasses in the oven at different temperatures. Figures 10 shows the size and color change of the specimens. According to these figures, as the temperature raised to 130°C, the industrial separator PP changed slightly.

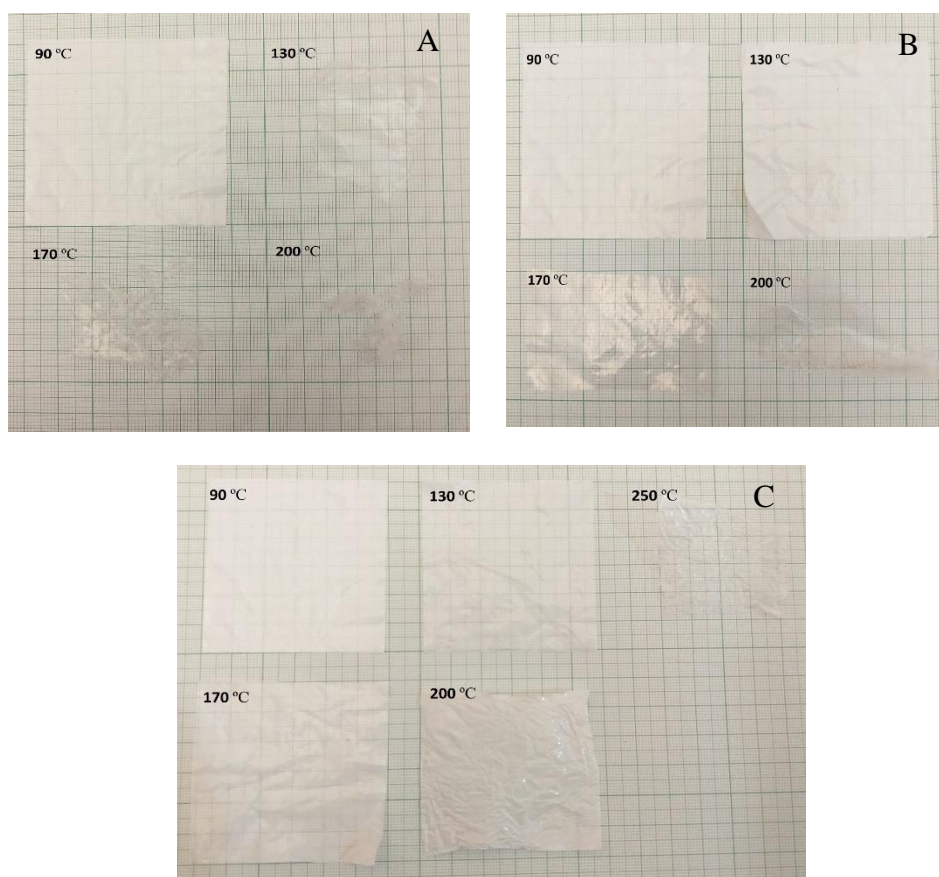


Figure 10. A) Images of the effect of temperature on the dimensional stability of PE separator; B) Images of the effect of temperature on the dimensional stability of PP separator; C) Images of the effect of temperature on the dimensional stability of PE/PET separator

By increasing the temperature to 170°C, the sample was completely melted and transparent. The PE sample melted at 130°C and lost its integrity; however, at 90°C for 30 minutes, it had shrinkage of less than 2%, which was in accordance with the expected properties. On the other

hand, with increasing temperature, PE/PET sample retained its integrity and exhibited less dimensional changes at mentioned temperatures despite PE melting after 120°C. The presence of a high melting temperature PET layer prevented PE thermal breakup and shrinkage and acted as a substrate for PE melt, where the rate of change was only about 10% at 200°C. As the temperature increased to the PET melting range, the separator became fully transparent and showed relatively high shrinkage.

The quantitative diagram for these images is shown in Figure 11. These results confirmed the efficacy of PE/PET separator in the field of shutdown safety, which was consistent with DSC test results.

To precisely check the shutdown characteristics and to determine the shutdown temperature, and the shutdown safety interval, the cells containing PE, industrial PP, and PE/PET separators were subjected to linear temperature increases, and their impedances were measured. The graph for this test is shown in Figure 12. According to this graph, impedance for PE separator increased sharply at a temperature of about 130°C, indicating that the battery was shutdown at this temperature. With the increase in temperature, a sharp decrease stemmed from short-circuiting due to the thermal shrinkage was observed beyond the separator limit at about 140°C. For industrial PP separators, shutdown occurred with a lower resistance value at about 160°C. This amount of resistance is not enough to stop the battery because the limit in the articles is about 800 to 1000 ohms. It also lost the mechanical integrity needed to prevent short-circuiting at about 180°C. For PE / PET bilayer separators, shutdown occurred at about 130°C with PE melting and a sharp increase in impedance. The short-circuit induced decrease occurred at a temperature of about 240°C with the onset of PET melting because by melting this component, the integrity of the separator film completely disappeared. A temperature difference of more than 100°C between shutdown and short circuit provides the safety needed to avoid potential hazards. These results are consistent with observations from the dimensional stability test and the DSC to an acceptable extent.

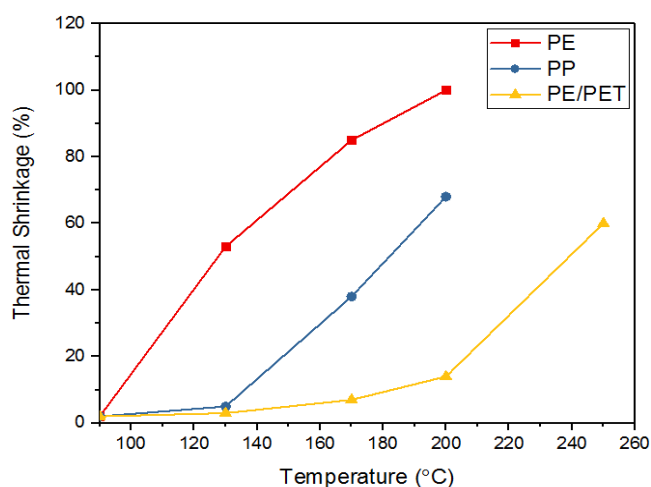


Figure 11. Thermal shrinkage curve of PE,PP and PE/PET separators

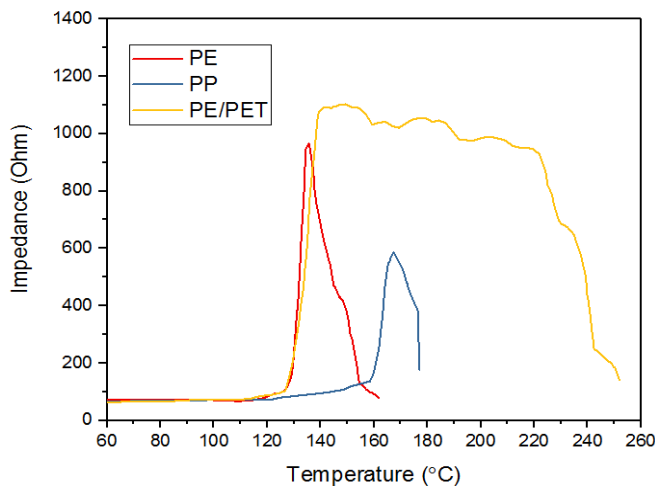


Figure 12. Results for shutdown properties of PE, PP and PE/PET separators

Table 4. Results of EIS test

Sample	Thickness (μm)	Ionic conductivity (mS/cm)	Resistance (Ω)
PP-Shenzhen	20	0.349	1.82
PE/PET	28	0.632	1.41

3.5. Electrochemical Performance of PE/PET separator

The ionic conductivity of the separators was obtained by measuring the impedance against the frequency and using the Eq. 4. Table 4 shows the results of this test. According to these results, the values obtained for the ion conductivity were in the same range of references [5,15,29]. The ionic conductivity of the bilayer sample was also higher than that of the industrial PP sample. The reason for this can be attributed to the greater compatibility of the bilayer sample with the electrolyte. As noted in Section 3.3, the presence of the PET layer increased the surface tendency to the electrolyte and increased electrolyte uptake, and this increased compatibility, decreased the resistance, and increased ionic conductivity.

The electrochemical stability range of the separators was investigated by linear scanning voltammetry (LSV) test. Figure 13 shows the graph of this test for industrial PP and PE/PET separators. In the LSV diagrams, the voltage corresponding to the onset of the increase in current density indicates the electrochemical stability limit of the electrolyte-soaked separator, where oxidative degradation occurs. According to the results, the increase in current density for PP and PE/PET samples were about 3.8 and 4.6 V, respectively. This is due to the absorption of the electrolyte by the bilayer separator and the reduction of the degradation of free electrolyte molecules in the battery. This result suggests that the PE/PET sample exhibits a wider electrochemical stability range than the industrial PP sample, meaning it will have greater stability and safety during operation. Given that almost all industrial electrodes have a

potential difference of less than 4.5 V, the electrochemical stability of the bilayer sample was sufficiently high for industrial application.

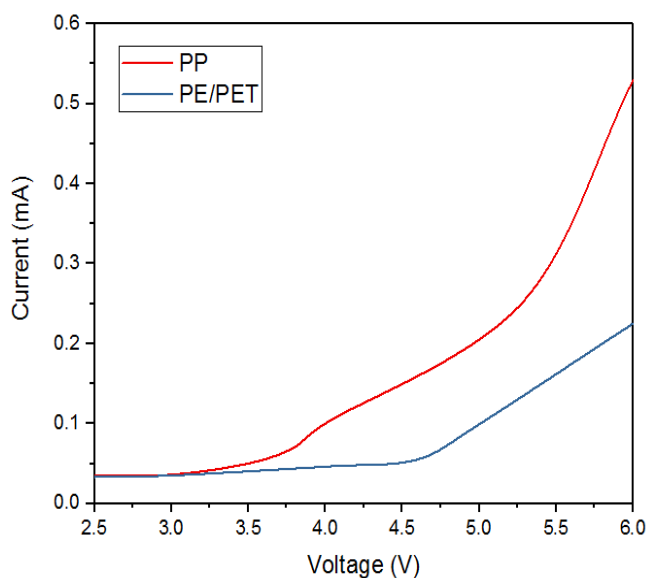


Figure 13. Linear sweep voltammetry of SS/PP/Li and SS/PE-PET/Li cells

Since the PE/PET bilayer separator showed higher ionic conductivity than the PP separator, it was expected to show better results in the battery performance test. To prove this hypothesis, the charge-discharge behavior of the cells containing PE/PET and PP separators was investigated using lithium and graphite as electrodes.

The performance of the test cells at different discharge speeds is shown in Figure 14. Compared to the industrial sample, PE/PET has shown better performance at all discharge rates due to higher ionic conductivity and greater electrolyte absorption ability.

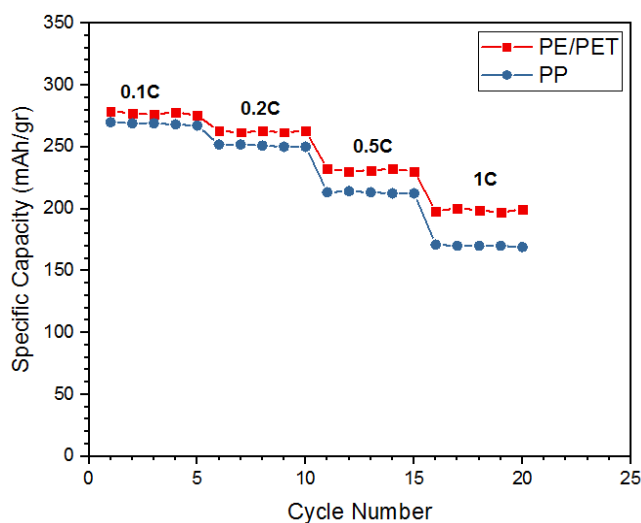


Figure 14. Rate capability of the cells with PP and PE/PET separators at different C-rates

Figure 15 shows the cycle performance diagram of cells containing PP and PE/PET separators. Both separators have shown relatively stable discharge capacity up to cycle 50 with a slight decrease. After 50 cycles, the test cell containing PE/PET separator had a discharge capacity of about 251mAh/gr, which is more than the test cell containing industrial PP separator (239 mAh/gr), which indicated the faster and easier transfer of lithium-ions between electrodes and lower interfacial impedance. Better discharge and cycle performance of the PE/PET bilayer sample demonstrated the potential of this separator for use in the industry.

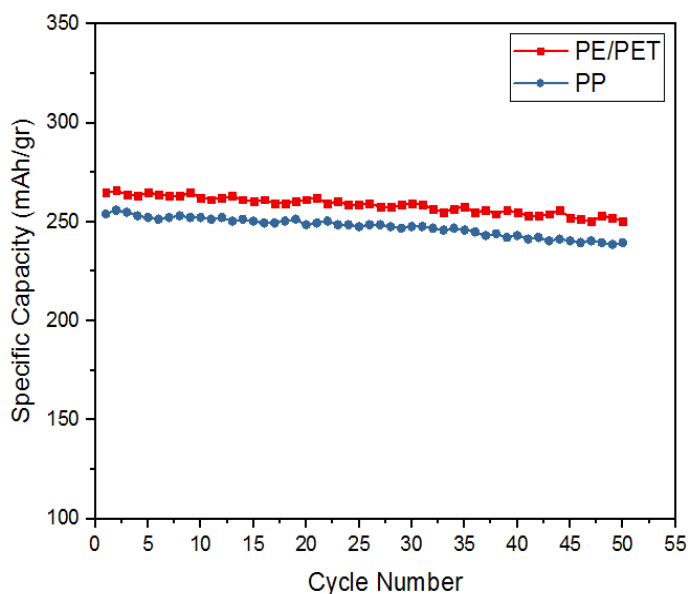


Figure 15. Cycle performance of the cells with PP and PE/PET separators at discharge rate of 0.2 C

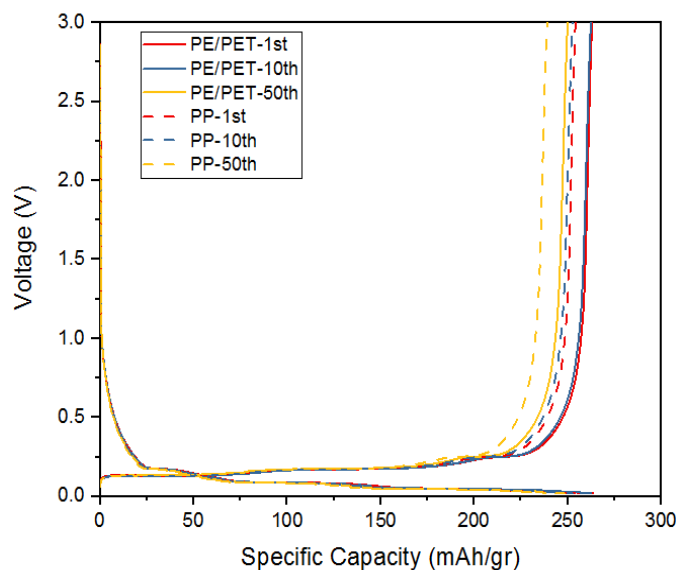


Figure 17. Charge and discharge profiles of the cells with PP and PE/PET separators at rate of 0.2 C

Figure 16 depicts 1st, 10th, and 50th charge and discharge profiles of cells assembled with PE/PET and PP separator, under a current density of 0.2 C and voltage range of 0.02 to 3 V. The curves are similar to what is observed for lithium-ion batteries in general, which implies a good contact between electrodes and separator. The typical flat-shaped profiles around 0.2V is consistent with graphite electrode. Also, the specific capacity of PE/PET bilayer separator is slightly higher than that of PP monolayer separator.

4. CONCLUSION

The fabrication of the PE separator by wet method resulted in a sample with optimum properties of 41% porosity, porous morphology proportional to the application, an average pore diameter of 22 nm, and a specific surface area of 39.3 g/m². To establish the safety of shutdown, the electrospinning method yielded favorable results, and the optimum conditions for polyethylene terephthalate (PET) electrospinning were obtained on the optimized sample produced in the previous step and resulted in the PE/PET bilayer separator fabrication. Necessary tests were performed to evaluate the performance of the PE/PET bilayer sample, and results were compared with similar tests corresponding to the industrial PP sample. The results of the electrolyte adsorption test showed that the bilayer PE/PET separator with about twice the electrolyte adsorption had better interaction with the electrolyte due to the higher polarity of PET and had better surface properties than PP. Shutdown test results confirmed with DSC results and dimensional stability test showed that the increase in impedance in the about 100°C melting temperature range of two components provided shutdown safety to avoid hazards. The results of the EIS test, while confirming the results of electrolyte adsorption, showed that with the presence of the PET layer, the ionic conductivity of the separator was higher than that of the industrial PP sample due to the increased affinity and surface compatibility with the electrolyte. The LSV test results showed that PE/PET sample had more electrochemical stability than the industrial PP sample (4.5V compared to 3.8V). The results of battery performance tests showed that the PE/PET separator had sufficient cyclic stability and had higher discharge capacity at similar rates than the industrial PP separator.

Acknowledgements

The authors are very thanks to University of Tehran, Center of Excellence in Electrochemistry for providing facilities support to bring about this work by major research project.

REFERENCES

- [1] C. J. Weber, S. Geiger, S. Falusi, and M. Roth, AIP Conf. Proc. 1597 (2014) 66.
- [2] Z. J. Zhang and P. Ramadass, "Lithium-Ion Battery Separators," in Lithium-Ion Batteries, New York, NY: Springer New York (2009) pp. 1–46.

- [3] K. Liu, Y. Liu, D. Lin, A. Pei, and Y. Cui, *Sci. Adv.* 4 (2018) eaat5168.
- [4] X. Huang, *J. Solid State Electrochem.* 15 (2011) 649.
- [5] H. Zhang, M. Y. Zhou, C. E. Lin, and B. K. Zhu, *RSC Adv.* 5 (2015) 89848.
- [6] H. Lee, M. Yanilmaz, O. Toprakci, K. Fu, and X. Zhang, *Energy Environ. Sci.* 7 (2014) 3857.
- [7] X. Yuan, H. Liu, and J. Zhang, "Lithium-ion batteries: Advanced materials and technologies," CRC Press (2011) pp. 1–428.
- [8] Z. Wang, W. Yu, and C. Zhou, "Preparation of polyethylene microporous membranes with high water permeability from thermally induced multiple phase transitions," *Polymer (Guildf)* vol. 56 (2015) pp. 535–544.
- [9] W. Chen, L. Shi, Z. Wang, Z. Zhuyi, Z. Jiefang, Y. Haijun, M. Xufeng, C. Mingming, S. Lining, and S. Yuan, *Carbohydr. Polym.* 147 (2016) 517.
- [10] M. S. Wu, P. C. J. Chiang, J. C. Lin, and Y. S. Jan, *Electrochim. Acta* 49 (2004) 1803.
- [11] M. Kim, G. Y. Han, K. J. Yoon, and J. H. Park, *J. Power Sources* 195(2010) 8302.
- [12] K. J. Kim, Y. H. Kim, J. H. Song, Y. N. Jo, J. S. Kim, and Y. J. Kim, *J. Power Sources* 195 (2010) 6075.
- [13] Y. Kim, W. Y. Lee, K. J. Kim, J. S. Yu, and Y. J. Kim, *J. Power Sources* 305 (2016) 225.
- [14] B. Xiong, R. Chen, F. Zeng, J. Kang, and Y. Men, *J. Memb. Sci.* 545 (2017) 213.
- [15] M. Waqas, S. Ali, C. Feng, D. Chen, J. Han, and W. He, *Small* 15 (2019) 1901689.
- [16] C. Martinez-Cisneros, C. Antonelli, B. Levenfeld, A. Varez, and J. Y. Sanchez, *Electrochim. Acta* 216 (2019) 68.
- [17] M. Baginska, B. J. Blaiszik, R. J. Merriman, N. R. Sottos, J. S. Moore, and S. R. White, *Adv. Energy Mater.* 2 (2012) 583.
- [18] D. Li, D. Shi, Z. Yuan, K. Feng, H. Zhang, and X. Li, *J. Memb. Sci.* 542 (2017) 1.
- [19] Z. Li, Y. Xiong, S. Sun, L. Zhang, S. Li, X. Liu, Z. Xu, and S. Xu, *J. Memb. Sci.* 565 (2018) 50.
- [20] W. Ji, B. Jiang, F. Ai, H. Yang, and X. Ai, *RSC Adv.* 5 (2015) 172.
- [21] L. Kong, B. Liu, J. Ding, X. Yan, G. Tian, S. Qi, and D. Wu, *J. Memb. Sci.* 549 (2018) 244.
- [22] X. Gao, W. Sheng, Y. Wang, Y. Lin, Y. Luo, and B. G. Li, *J. Appl. Polym. Sci.* 132 (2015) 1.
- [23] S. H. Tabatabaei, P. J. Carreau, and A. Ajji, *J. Memb. Sci.* 345 (2009) 148.
- [24] J. Hao, G. Lei, Z. Li, L. Wu, Q. Xiao, and L. Wang, *J. Memb. Sci.* 428 (2013) 11.
- [25] J. L. Shi, H. Li, L. F. Fang, Z. Y. Liang, and B. K. Zhu, *Chinese J. Polym. Sci. (English Ed.)* 31 (2013) 309.
- [26] M. J. Park, and C. K. Kim, *J. Memb. Sci.* 449 (2014) 127.
- [27] H. Liao, H. Hong, H. Zhang, and Z. Li, *J. Memb. Sci.* 498 (2016) 147.

- [28] Y. Li, H. Pu, and Y. Wei, *Electrochim. Acta* 264 (2018) 140.
- [29] V. Deimede and C. Elmasides, *Energy Technol.* 3 (2015) 453.
- [30] “Celgard Datasheets.” [Online]. Available: <https://www.celgard.com/literature>.
- [31] J. Y. Song, Y. Y. Wang, and C. C. Wan, *J. Electrochem. Soc.* 147 (2000) 3219.
- [32] P. Arora, Z. J. Zhang, S. Lakes, and N. Carolina, *Chem. Rev.* 104 (2004) 4419.